[American Journal of Science, Vol. 321, November, 2021, P. 1285–1307, DOI 10.2475/09.2021.01]

American Journal of Science

NOVEMBER 2021

EARLY CRETACEOUS SOLAR CYCLES RECORDED IN LACUSTRINE LAMINATIONS IN NORTH CHINA

XING TIAN*,**, YUAN GAO*,**,†, TYLER KUKLA***, OLAF LENZ§, HE HUANG*,**, DANIEL E. IBARRA§§,§§§, SHOULIANG SUN‡, and CHENGSHAN WANG*,**,†

ABSTRACT. Solar cycles are important moderators of the Earth's global climate system. Although modern-day solar cycles are well known, they have been less studied over geological time. High-resolution records such as varves have been previously used for reconstructing solar cycles from the Paleoproterozoic through Quaternary. In this paper, very fine (<1 mm) sedimentary laminations of the Early Cretaceous Yixian Formation in Xiushui Basin were studied in Northern Liaoning Province, North China. Two different microfacies of the striped shale in the Third Member of the Yixian Formation were identified. These include the light-gray to gray siltstone (Mf 1) and the gray to black organic-rich mudstone (Mf 2). Laminations of Mf 2 are mainly made of biofilms. Sub-millimeter scaled couplets of biofilm and siliciclastic-rich sublamina record seasonal growth and withering of microbial mats during the warm season (summer) and cold season (winter), respectively. Evolutionary spectral analyses of three binary rank series (the binary boxcar series, triangle series, and mid-point-triangle series), varve couplet thickness and gray scale image data (gray data) show multiple periodicities consistent with solar cycles, including the robust Schwabe sunspot cycle (10.0–10.6 year) and solar Bruckner cycle (31.0–40.6 year), and relatively weaker signals for the solar Hale cycle (21.9 year) and 16.5-year solar cycles that have been linked to solar magnetic activity. Solar cycles recognized in this paper indicate the total solar irradiance (TSI) influenced microbial mat growth in the Early Cretaceous in North China. Further, we extend our new record with a compilation of varve-recorded sunspot cycles throughout geological time to show that the 11-year Schwabe sunspot cycle and the 22-year Hale cycle have persisted since the Paleoproterozoic.

Key words: Early Cretaceous, Yixian Formation, biofilm, sunspot cycle, lacustrine varves

INTRODUCTION

The sun is the ultimate energy source to the Earth surface, and periodic changes in solar radiation fundamentally control Earth's climate cycles (Lean and Rind, 2001; Gray and others, 2010; Biktash, 2019,). The most prominent solar cycles are the 11-

* State Key Laboratory of Biogeology and Environmental Geology, China University of Geosciences, Beijing 100083, China
** School of the Earth Science and Resources, China University of Geosciences, Beijing 100083, China
*** Department of Geological Sciences, Stanford University, Stanford, California 94305, USA
§ Senckenberg Research Institute and Natural History Museum Frankfurt, 60325 Frankfurt am Main, Germany
§§ Department of Earth and Planetary Science, University of California, Berkeley, California 94720 USA
§§§ Institute at Brown for Environment and Society and the Department of Earth, Environmental and Planetary Science, Brown University, Providence, Rhode Island, 02912 USA
‡ Shenyang Center of Geological Survey, China Geological Survey, Shenyang 110034, China
† Corresponding authors: yuangao@cugb.edu.cn, chshwang@cugb.edu.cn

year Schwabe cycle (Schwabe, 1844), the 22-year Hale cycle (Hale, 1908; Hale and others, 1919), and the 88-year Gleissberg cycle (Gleissberg, 1939), of which solar variances are largely characterized by sunspots. Sunspots appear as dark patches on the Sun where intense magnetic fields loop up through the surface from the deep interior (Hathaway, 2015). The 11-year Schwabe sunspot cycle is characterized by the rise and fall in the total number and surface area of sunspots (Schwabe, 1844), the 22-year Hale cycle is characterized by the changing polarity of sunspots and the solar magnetic fields (Hale, 1908), while the 88-year Gleissberg cycle is a long-period fluctuation of the number of sun-spots (Gleissberg, 1939). Other solar cycles, like the Bruckner cycle, are less well known. When the Bruckner cycle was first discovered its periodicity was defined as 34.8 ± 0.7 years, but later work has modified its duration to 30 to 45 year (Sazonov, 1979). Raspopov and others (2000) interpreted this cycle to be the result of the nonlinear effect of solar activity and variability on atmospheric process.

Modern total solar irradiance (TSI) is considered to be the main cause of the solar contribution to global climate change (Gray and others, 2010; Lockwood, 2012; Solanki and others, 2013), and TSI is proved to be in-phase with sunspot cycles (Gray and others, 2010; Solanki and others, 2013). Although the sunspot cycles are well known, they have only been sporadically reported from the Proterozoic to Cenozoic, primarily because high-resolution sedimentary records like varves (annually laminated sediments) and fossilized tree rings are rare in sedimentary rocks (Thackeray, 2002; Ojala and others, 2012; Zolitschka and others, 2015; Schimmelmann and others, 2016; Luthardt and Rößler, 2017), thus limiting our understanding of sunspot periodicities and their persistence through geological time (Andrews and others, 2010; Luthardt and Rößler, 2017; Li and others, 2018).

Varves are annually deposited lamina in both terrestrial and marine settings (Francus and others, 2013; Zolitschka and others, 2015; Schimmelmann and others, 2016) that can be categorized into four different types by the dominating sedimentary component: i) clastic varves are composed of siliciclastic particles; ii) biogenic varves result from biological production of organic matter (such as biofilm laminae) and biomineralization; iii) endogenic (minerogenic) varves are formed via chemical precipitation of minerals; and iv) mixed varves are combinations of clastic, biogenic and endogenic sediments (Anderson and Dean, 1988, Zolitschka and others, 2015). Sunspot cycles have been reported from varves in the Pre-Quaternary/deep-time (table 1), including: Paleoproterozoic rhythmically deposited argillites from a glacial lacustrine environment (Hughes and others, 2003); Mesoproterozoic marine carbonate biolaminites (Tang and others, 2014) and lacustrine deposits (Andrews and others, 2010); Neoproterozoic laminated limestone (Korn, and Martin, 1951) and carbonate biolaminites (Li and others, 2018), both marine in origin; Devonian non-glacial varves (Andrews and others, 2010); Carboniferous biogenic marine varves (Algeo and Woods, 1994) and glacial marine clastic varves (Milana and Lopez, 1998); as well as other examples summarized by Li and others (2018). The Cretaceous Period is a critical time interval in Earth's history for shaping our understanding of climate variability during past greenhouse conditions and our ability to forecast future climate change (Wang and others, 2013; Tierney and others, 2020). Although sunspot related varve records were reported from the Late Cretaceous Arctic Ocean (Davies and others, 2012), no similar work has been carried out in the Early Cretaceous in either terrestrial or marine settings, and how solar cycles affect climate and ecosystems in greenhouse states remains uncertain.

In the Early Cretaceous, multiple lacustrine basins developed in the modern Liaoning Province of North China, in which the world-famous Jehol Biota is preserved (Zhou and others, 2003; Chang and others, 2006; Sha, 2007; Jiang and others, 2012;

TABLE 1

Examples of Schwabe sunspot cycle, solar Hale cycles and Gleissberg cycles recorded in the Pre-Quaternary/deep-time varves.

Num.	Geological Era and Periods	Countries	Depositional environments	Varve types	Periodicities (year)	Type of cycles	References
1	Pliocene	Spain	lacustrine	Biogenic varves /pollen layer	12	Schwabe	Gauthier and Muñoz (2009); Muñoz and others (2002)
2	Miocene-Pliocene	America	sinkhole lake	Clastic varves/clay and organic layer	12, 24	Schwabe and Hale	Shunk and others (2008)
3	Miocene	Mediterranean	marine (restricted lagoon)	Mixed varves/clay and calcite laminae	10	Schwabe	Cosentino and others (2005)
4	Eocene	Germany	maar lake	Biogenic varve/algal and terrigenous layer	10-11, 17-26	Schwabe and Hale	Lenz and others (2010)
5	Late Cretaceous	America	marine (forearc basin)	Biogenic varves /diatomaceous layer	10.3-10.8	Schwabe	Davies and others (2012)
6	Early Cretaceous	China	lacustrine	Biogenic varves /biofilms	10.0-10.6, 21.9	Schwabe and Hale	This study
7	Late Jurassic	America	gulf coast	Endogenic (minerogenic) varves/carbonate laminae	12, 24	Schwabe and Hale	Heydari and others (1997)
8	Jurassic	America	non-marine /saline paralic	Endogenic (minerogenic) varves/ limestone and gypsum layer	13, 20, 78, 179, 235	Schwabe, Hale, Gleissberg, and Suess/De Vries cycle	Anderson and Kirkland (1960); Dmitriev and others (2016)
9	Permian-Carboniferous	Brazil	glacial marine	Clastic varves/siliciclastics layer	12.4, 24.4	Schwabe and Hale	Ernesto and Pacca (1981)

TABLE 1
(continued)

Num.	Geological Era and Periods	Countries	Depositional environments	Varve types	Periodicities (year)	Type of cycles	References
10	Carboniferous	Argentina	glacial marine	Clastic varves/siliciclastics	12, 24-26	Schwabe and Hale	Milana and Lopez (1998)
11	Carboniferous	American	marine (central basin)	Biogenic varves/clay and organic layer	23±2, 70±5	Hale and Gleissberg	Algeo and Woods (1994)
12	Devonian	Scotland	non-glacial lake	Mixed varves/organic, carbonate, and siliciclastic layer	8.6-13.7, 19.6-22.7	Schwabe and Hale	Andrews and others (2010)
13	Neoproterozoic	Namibia	marine	Mixed varves/banding of dolomites and shales	11.4	Schwabe	Korn and Martin (1951)
14	Neoproterozoic	China	marine (lower shoreface)	Biogenic varves/biolaminites	10-11.4, 18.9-25.6	Schwabe and Hale	Li and others (2018)
15	Mesoproterozoic	Scotland	non-glacial lake	Clastic varves /silt-clay and organic couplets	9.2-10.6	Schwabe	Andrews and others (2010)
16	Mesoproterozoic	China	marine (restricted subtidal lagoon)	Biogenic varves/biolaminites	9.0-11.7, 19.7-21.4	Schwabe and Hale	Tang and others (2014)
17	Paleoproterozoic	Canada	glacial lake	Clastic varves/siliciclastics layer	9.9-10.7, 14.3	Schwabe	Hughes and others (2003)

Pan and others, 2012). Laminations have been well studied and varves have been reported from the Early Cretaceous lacustrine deposits in adjacent areas (Zhang and Sha, 2012; Hethke and others, 2013). Zhang and Sha (2012) recognized three different kinds of laminations from the Sihetun Fossil site, these laminations exist in black mudstone, gray-pale to gray-greenish mudstone and shale, respectively. Based on lamination patterns (couplets or triplets), the average varve thicknesses are approximately equal to the annual sedimentation calculated by other dating methods (Zhu and others, 2007; Chang and others, 2009). Therefore, it has been proposed that most of the laminations are varves (Zhang and Sha, 2012). After describing detailed sedimentological characteristics of the laminations in the Sihetun paleolake, Hethke and others (2013) summarized 6 different kinds of micro-lithofacies, including allochthonous, siliciclastic laminae (Mf 1), chrysophycean cyst accumulations (Mf 2), tuffaceous silt (Mf 3), lacustrine chemical precipitates (Mf 4), tuff (Mf 5) and normal graded, sandy to silty siliciclastics (Mf 6), of which Mf 2 and Mf 4 are varves. However, spectral analysis has not yet been conducted to determine the origin of the rhythms in these varves.

Here we present a detailed sedimentological study of lacustrine laminations from borehole sediments of the Early Cretaceous Yixian Formation in the Xiushui Basin, Northern Liaoning Province, and demonstrate they are varves similar to those reported by Zhang and Sha (2012) and Hethke and others (2013). We further carry out power spectral analyses and discover periodicities consistent with solar activities and interannual climate cycles. This paper discusses the paleoclimatic and paleoenvironmental significance of the observed laminations and cycles with emphasis on the persistence of solar cycles through geological history.

GEOLOGIC SETTING

The Xiushui Basin is located in the Northern Liaoning Province, North China. It is a Mesozoic rift basin overlying the Precambrian basement. This basin is about 34 km long and 15 to 25 km wide, covering an area of 710 km^2 (fig. 1A; Ding and others, 2017). Geomagnetic data show that the paleolatitude of NE China during the Early Cretaceous is similar to today (Zhu and others, 2002). Tectonic evolution of this basin had 4 stages: initial basement formation, early extensional fault depression, volcanic eruption, and differential uplift and erosion (Ding and others, 2019). From north to south of the basin exits three depressions: the Woniushi sag, the Dengshibu sag and the Dongsheshan sag (fig. 1A; Li and others, 2019b).

The Xiushui paleolake was a continental freshwater lake during the deposition of the Early Cretaceous Yixian Formation (Li and others, 2019b). Permian-Jurassic granite from northeast and east of the basin contribute the majority of the sediment provenance (Cao, ms, 2013, Li and others, 2019b). The sedimentary strata of the Yixian Formation was formed during a period of intermittent volcanism (fig. 1C) and has constituted the main target interval of oil and gas exploration (Ding and others, 2019). Based on spore-pollen assemblages, the upper part of the Yixian Formation was roughly limited to Valanginian-Hauterivian (Ding and others, 2017). Previous work demonstrates that deep and reduced lake environmental conditions promoted deposition of the dark mudstone in the Third Member of the Yixian Formation (Li and others, 2019b).

LF-D1 borehole (fig. 1A) is the deepest and most comprehensive well in the Dengshibu sag in Xiushui Basin (Li and others, 2019b). The Yixian Formation recovered by LF-D1 borehole (fig. 1) is 1800 m and the core recovery was more than 98 %. The sedimentary rocks of the core are mainly mudstone and siltstone, sandwiched between igneous rocks. The total length of the sedimentary rocks of the Third

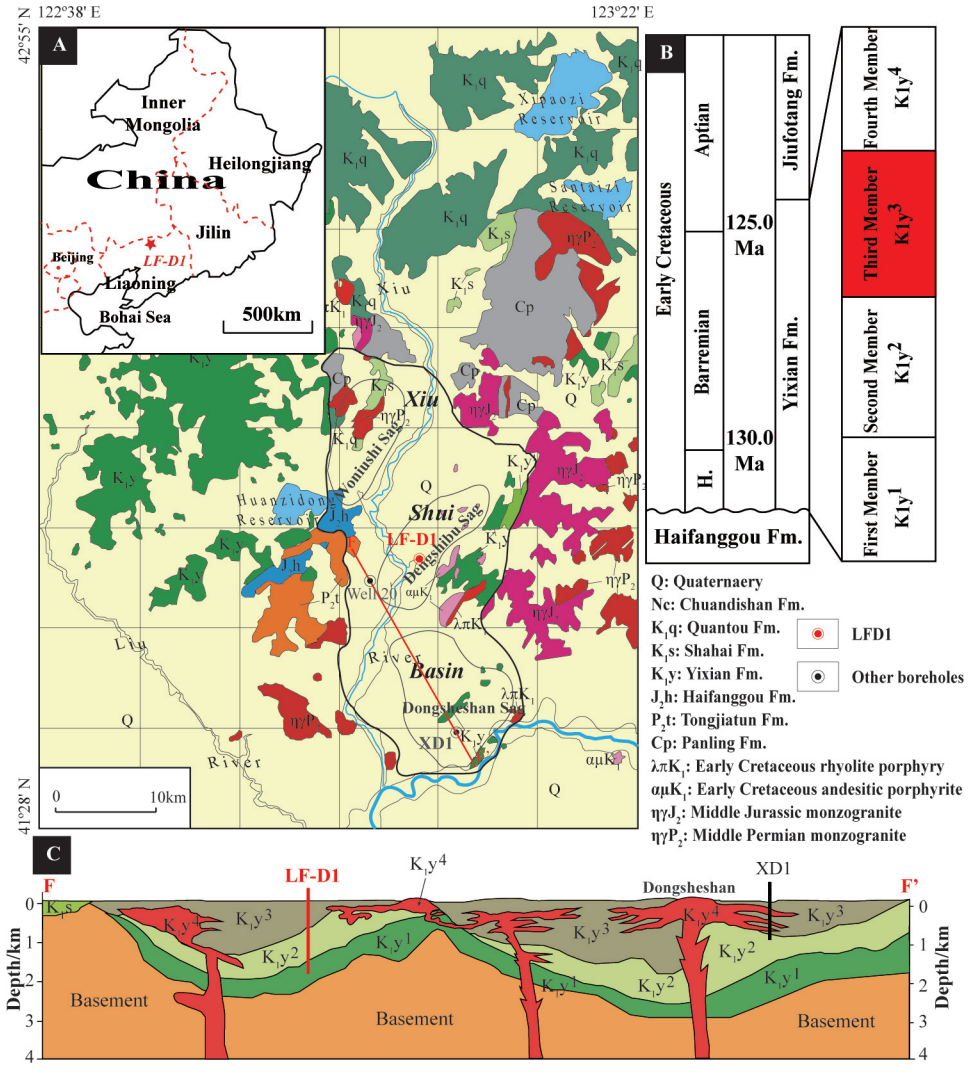

Fig. 1. The Xiushui Basin of the Northern Liaoning, NE China, and its geographic extent (A) the sketch of the Northeastern China showing the relative location of the LF-D1 and the Sihetun fossil site, and the geological sketch map of the Xiushui basin and the sites of the LF-D1 boreholes in the basin; (B) stratigraphic column of the Yixian Formation; (C) lithostratigraphic framework along the F-F' cross section in A. Modified from Chen and others (2016), Ding and others (2017, 2020), Li and others (2017), Jiang and others (2012), Yao and others (2018), and Zhang and Sha (2012).

Member of the Yixian Formation is 280 m thick, with dark-colored fine-grained sedimentary rocks more than 128 m (fig. 2).

MATERIALS AND METHODS

Observations of the LF-D1 core drilled in the Xiushui basin, Northern Liaoning (fig. 2) show that laminations are well preserved in the striped, fine-grained sedimentary rocks/shales. Laminations can be observed by the naked eye. The most well-laminated fine-grained sedimentary rocks of the cores are found within the Third Member of the Yixian Formation (K_1y^3). For this study, samples of K_1y^3 from LF-D1

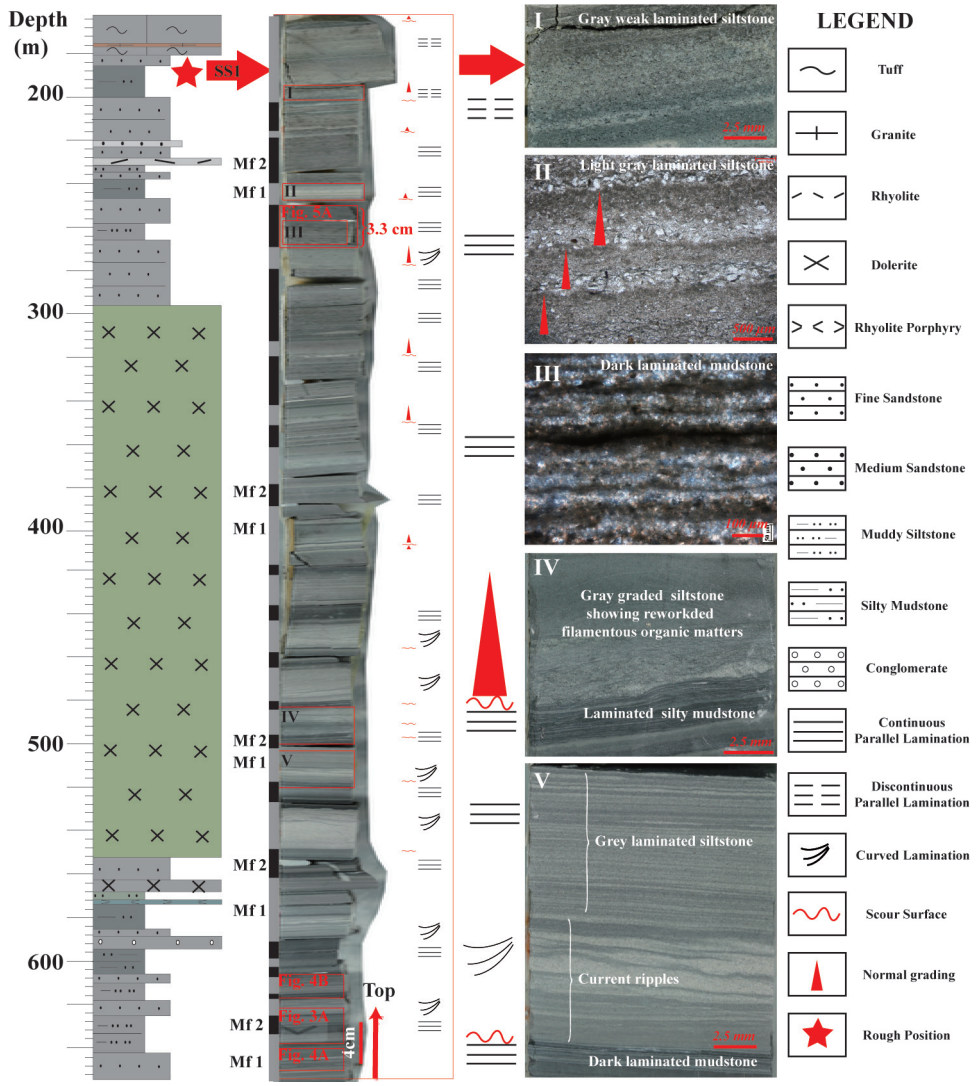

Fig. 2. Sedimentary structures, and core photos of the striped shale from the Third Member of the Yixian Formation. Red rectangles show the rough areas of figures 3, 4, and 5.

spanning depth of 181.04m to 182.06m (SS1) were continuously sampled, pasted, carefully spliced and polished into core slabs to ensure complete sections and clear surfaces (fig. 2). High quality photos of these core slabs were taken. All of the samples were investigated with thin sections under optical microscope.

The well-laminated samples (fig. 2) were further studied using a Polarizing Microscope, Scanning Electron Microscope (SEM), and Cathode Luminescence (CL). Thin sections were used to study the micro-fabrics and components of the laminations, with a Polarizing Microscope LV100N POL for high magnification. Thin sections were continually and seamlessly spliced together into a high-resolution photo with Adobe Illustrator Program. Following this, gray scans were carried out in Image J (https://imagej.nih.gov/ij/download.html). Samples for SEM experiments were

coated with ~10-nm-thick platinum for electric conduction before analysis. The SEM measurements were carried out on a JEOL JSM-6700F SEM at KYKY Technology Co., LTD. Cathode Luminescence (CL) experiments of the laminations were conducted with a CL 8200 MK5-2 at State Key Laboratory of Biogeology and Environmental Geology, China University of Geosciences (Beijing).

Of the 1.02 m sections described above, a 3.3 cm long varved interval (362 laminar couplets, fig. 2) was selected and used for data acquisition and subsequent spectral analysis. We established a high-resolution binary data series by assigning a "rank" of 1 and 0 for the siliciclastic-rich sublamina and organic-rich sublamina, respectively. Following this, binary data were further processed into triangle and mid-point triangle series (detailed procedures are outlined in: Yao and others, 2015; Yao and Hinnov, 2019). We also measured the lamina thicknesses in thin sections and acquired gray data with the same sample. Evolutionary spectral analysis of the data series were carried out with the Acycle software (Li and others, 2019a), which provides reproducible and objective methods for analyzing paleoclimate signals. Spectral analysis methods in Acycle are similar to those described by others (Weedon, 2003; Meyers, 2014). Apart from the binary rank series, the varve couplet thickness and the gray data set of the 3.3 cm lithology were also tested by Acycle to confirm the stability and robustness of the main peak signals.

DESCRIPTION AND INTERPRETATION OF THE STRIPED SHALES

Based on rock color and composition, two different microfacies (Mfs) of the striped shales (figs. 2 and 3) are recognized: i) light-gray to gray siltstone (Mf 1), and ii) gray to black organic-rich mudstone (Mf 2). Figures 2 and 3 show the frequently alternating thin layers of siltstone and mudstone that, together, comprise the striped shales. Details of the two microfacies are described below.

MF 1: THE LIGHT-GRAY TO GRAY SILTSTONE

Description

Mf 1 (fig. 4) is primarily composed of siliciclastic layers characterized by light-gray to gray siltstone in striped shale (fig. 2). It can be parallel laminated (fig. 3B), cross laminated, and massive (fig. 2). It can also form weak normal graded siltstone (fig. 2) and rhythmites (fig. 4A). The normal grading contains floating filamentous organic matter (figs. 2 and 4A). Varying amounts of quartz (the main component) and organic matter result in dark and light laminae (fig. 3B). Detrital quartz floating in the muddy matrix, and the organic clasts are parallel to lamina surfaces. Different directions of current ripples (fig. 4B) exist above the parallel laminations. Mf 1 and Mf 2 are easy to distinguish because they have clear boundaries and appear as alternating, thin-layered mudstone and siltstone (fig. 3A), respectively.

Interpretation

We interpret this lithofacies as event layers, such as deposits from turbidity currents and storms. The existence of sharp or micro-erosional basal contacts (figs. 2 and 4) indicate strong hydrodynamic conditions, an observation very common in turbidites (Bouma, 1964; Shanmugam, 2021). In turbidity currents, waning flows result in weak normal grading (Bouma, 1964), and the hydrodynamic strength determines whether there are basal erosional surfaces or floating objects (Bouma, 1964; Yang and others, 2020; Shanmugam, 2021). Structureless or massive siltstone can be formed by direct suspension fallout (Bouma, 1964). Parallel laminations and current ripples (fig. 4) are deposited by dilute turbidity currents and tend to be the products of traction (Stow and Piper, 1984; Talling and others, 2012; Spychala and others, 2017). In sum,

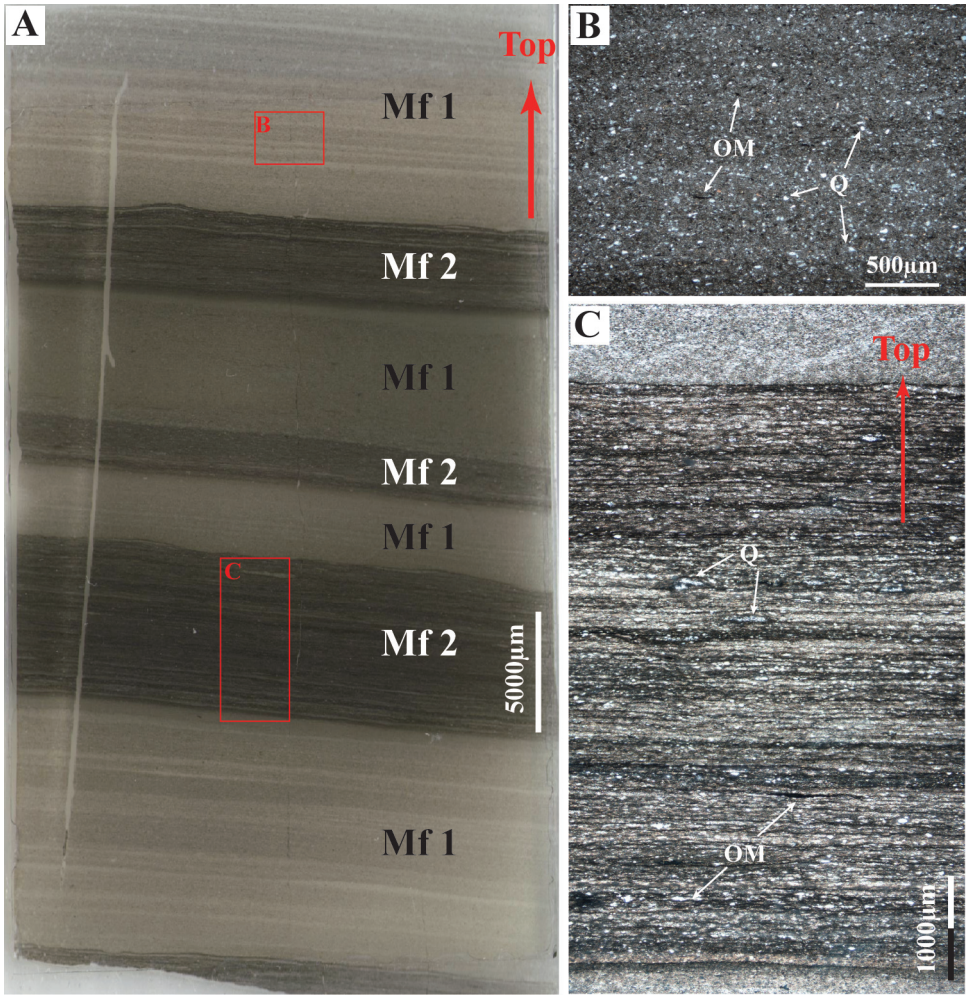

Fig. 3. Microfacies of the striped mudstone in LF-D1 (fig. 2). A) Macrophoto of the striped shales. The red rectangles show the position of B and C; B) Laminated light-gray to gray siltstone (Mf 1), which are mainly composed of terrigenous components, such as quartz, clay and amorphous organic matter (algal debris?), crossed polarized. C) Thin sections of the laminated gray-black organic-rich mudstone (Mf 2). The laminae are horizontally continuous, silt lenses and floating terrigenous clasts are wrapped. Q: Quartz; OM: Organic Matter.

these observations demonstrate that Mf 1 could not be deposited in a quiet water column, instead, it is most likely to be transported and deposited by turbidity currents.

Mf 2: The Gray to Black Organic-Rich Mudstone

Description

Rhythmic laminations of the Mf 2 are stacks of laminar couplets of siliciclastic-rich sublaminae and organic-rich sublaminae. Based on the regularity of the organic-rich sublaminae, we found two different types of Mf 2: (1) the irregular laminated organic-rich mudstone (Mf 2-1; fig. 3C), and (2) the regular laminated organic-rich mudstone (Mf 2-2; fig. 5). The regularity of laminar couplets of Mf 2-2 makes it

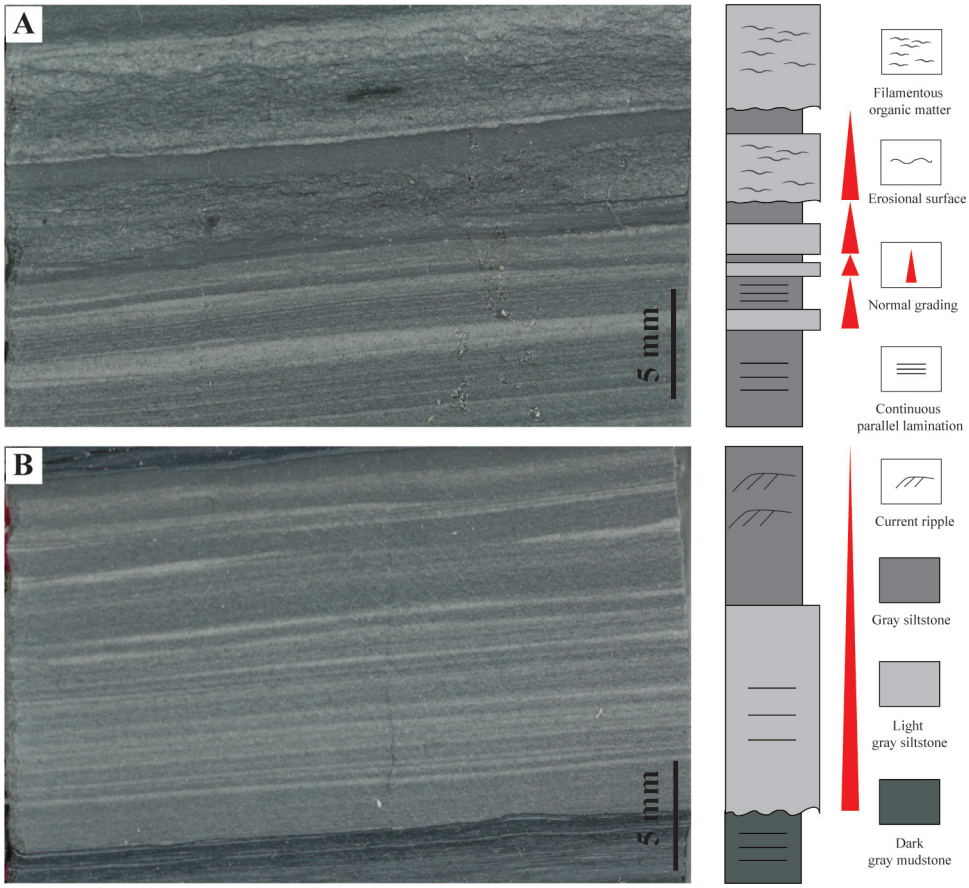

Fig. 4. The light-gray to gray siltstone (Mf 1). A) Macrophoto of the Mf 1 showing floating filamentous organic matter, micro-erosional surfaces, parallel lamination and normal grading; B) Macrophoto of the Mf 1 showing even distributed silty organic matter, micro-erosional surfaces, parallel lamination, current ripple and normal grading.

countable, and thus Mf 2-2 was used for further petrological and spectral analysis in this paper.

Mf 2-1 is deposited as a gray, irregular laminated organic-rich mudstone (fig. 2). It is characterized by slightly disturbed, very fine laminations (figs. 3C). Mf 2-1 is fragile and present as interlayers in the striped shale. The organic laminae are wavy-crinkled. The thickness and texture of the siliciclastic-rich sublaminae and organic-rich sublaminae are very thin (58.6 μm, n=52) and irregular (fig. 3C). Mf 2-1 contains lots of floating sand-sized quartz and silt lenses (fig. 3C).

Mf 2-2 is deposited as a brownish-gray to black, well laminated organic-rich mudstone (fig. 2). It is not easy to observe with magnifying glasses in the core (figs. 2 and 5A). However, viewed in thin sections (fig. 5), the laminae appear as densely packed laminar couplets that consist of alternating dark colored organic-rich sublamina and light colored siliciclastic-rich sublamina. Similar to Mf 2-1, the organic lamina of Mf 2-2 contains organic matter with a filamentous network (fig. 5), however the organic-rich laminae of Mf 2-2 include floating silty organic matter (figs. 5 and 6). The thickness of the Mf 2-2 laminar couplets usually amounts to tens of micrometers, minor couplets are hundreds of micrometers, with an average thickness of ~90.4 μm

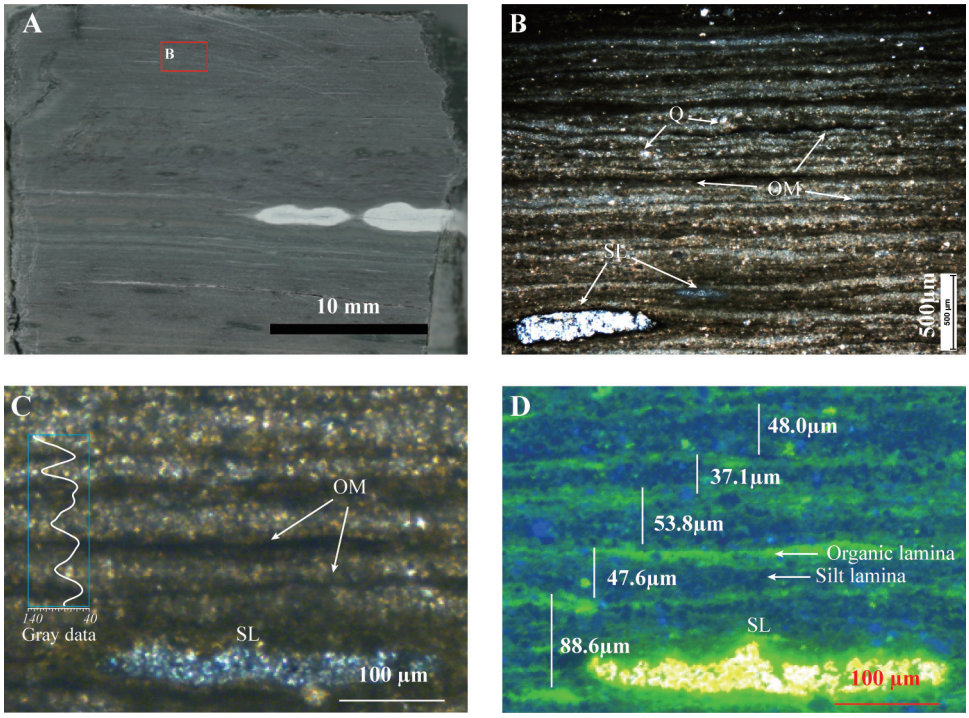

Fig. 5. Cathode Luminescence (CL) of the gray to black organic-rich mudstone (Mf 2). A) Macrophoto of the Mf 2 showing laminations observable by naked eye, and the position of B; B) Mf 2 showing the couplet of siliciclastic-rich sublamina and organic-rich sublamina, and quartz (Q) and silt lenses (SL) trapping, plane polarized light; C) Mf 2 showing filamentous features of organic matter (OM) in the organic-rich sublamina, and silt lenses trapped, as well as the great relationship between gray data and varve couplets, plane polarized light; D) Cathode Luminescence (CL) of C, the organic-rich sublaminae display yellow-green fluorescence, while the siliciclastic-rich sublaminae have no fluorescence.

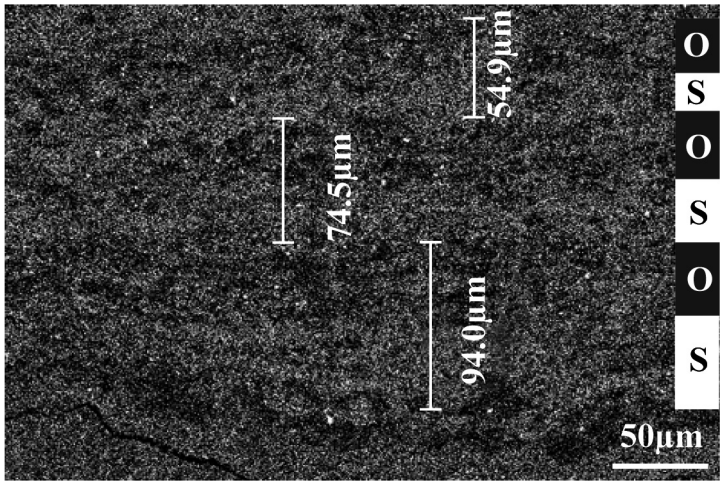

Fig. 6. Scanning electron microscope (SEM) of the regular laminated organic-rich mudstone (Mf 2-2), showing floating silty organic matter. O: Organic rich sublamina, S: Siliciclastic-rich sublamina.

(n=362). The siliciclastic-rich sublaminae are usually thinner than the organic-rich sublaminae. Mf 2-2 also contains numerous floating sand-sized quartz and silt lenses, which are composed of quartz and organic matter (fig. 5D).

Interpretation

The presence of filamentous network structures of the organic-rich sublaminae (figs. 3C and 5), quartz, silt lenses trapping or bundling (figs. 3C, 5, and 6), and mechanical destruction of filamentous organic matters (figs. 2 and 4A) provide robust evidence for a microbial mats origin for Mf 2, as these features are commonly associated with cyanobacterial mats (Schieber, 1986; Schieber and others, 2007; Noffke, 2010; Li and others, 2018). Modern and historical microbial mats occur mostly in intertidal and subtidal environments (Schieber, 1986; Schieber and others, 2007; Noffke, 2010; Li and others, 2018). We found no evidence for exposure to the surface (for example, mudcracks), so it is likely that the biofilms analyzed in this paper were deposited under subtidal environments or deeper.

As shown in figure 2, Mf 2-1 tends to be preserved in the lower part of the sample, with more intervals of light-gray to gray siltstone (Mf 1), while Mf 2-2 in the upper part has greater mud content (fig. 2), suggesting that Mf 2-2 may be deposited in deeper water. The organic matter in Mf 2-2 is sometimes filamentous, but most laminae are dotted (figs. 5 and 6). The 'rainy' organic matter (figs. 5 and 6) is likely deposited by accumulation of organic matter through fragments of previous *in situ* microbial mats swept into the quiet basin (Schieber, 1986; Schieber and others, 2007). In sum, the biofilms in Mf 2-1 were dominated by benthic microbial mats, while Mf 2-2 may be deposited mainly by suspension in a deeper water column.

LAMINA DURATION AND SEDIMENTARY MODEL OF THE STRIPED SHALE

Determing the duration of each lamina is critical for interpreting the laminae periodicities. Despite a long history of varve research (Gilbert, 1895; de Geer, 1912), the duration of lamina or laminar couplets is still ambiguous because the formation may be responding to different-order, periodic and non-periodic changes (Arenas and Jones, 2017). Several lines of evidences here point to an annual nature of the laminar couplets in Mf 2-2.

First, Mf 2-2 laminations are thin (90.4 μm) and rhythmic, consistent with periodic deposition and in contrast with the event layer deposits of Mf 1 that indicate stochastic deposition (Tang and others, 2014; Li and others, 2018). The average thickness of Mf 2-2 is 90.4 μm (characterized by 362 laminar couplets in a 3.3 cm-long interval). According to previous lacustrine varve databases (Ojala and others, 2012; Zolitschka and others, 2015), the average thicknesses of different lacustrine varves varies from 70 to 27300 μm, and over 65 % of the varve thickness falls into 0 to 1500 μm.

Second, biofilm growth tends to vary seasonally with changes in total solar irradiance and temperature (Villbrandt and others, 1991; Pinckney and others, 1995; Hawes and others, 2014; Ma and others, 2017). The laminar couplets of Mf 2-2 consist of similar biofilms such that one couplet likely reflects one year (a warm and a cold season). Studies of modern microbial mats support this notion. For example, over 3 years of observation, Villbrandt and others (1991) found that nitrogen fixation and photosynthetic activities of cyanobacterial mats were highest in spring and summer, and biofilms/microbial mats initiated in higher irradiance and warmer years tend to be thicker than those from lower irradiance and colder years (Villbrandt and others, 1991; Hawes and others, 2001; Sutherland and Hawes, 2009; Hawes and others, 2016). Further, the total solar irradiance and temperature vary abruptly between summer and winter in the mid-latitudes (Howard and others, 1998; Sutherland and Hawes, 2009; Hawes and others, 2016). In modern summertime, solar irradiance and

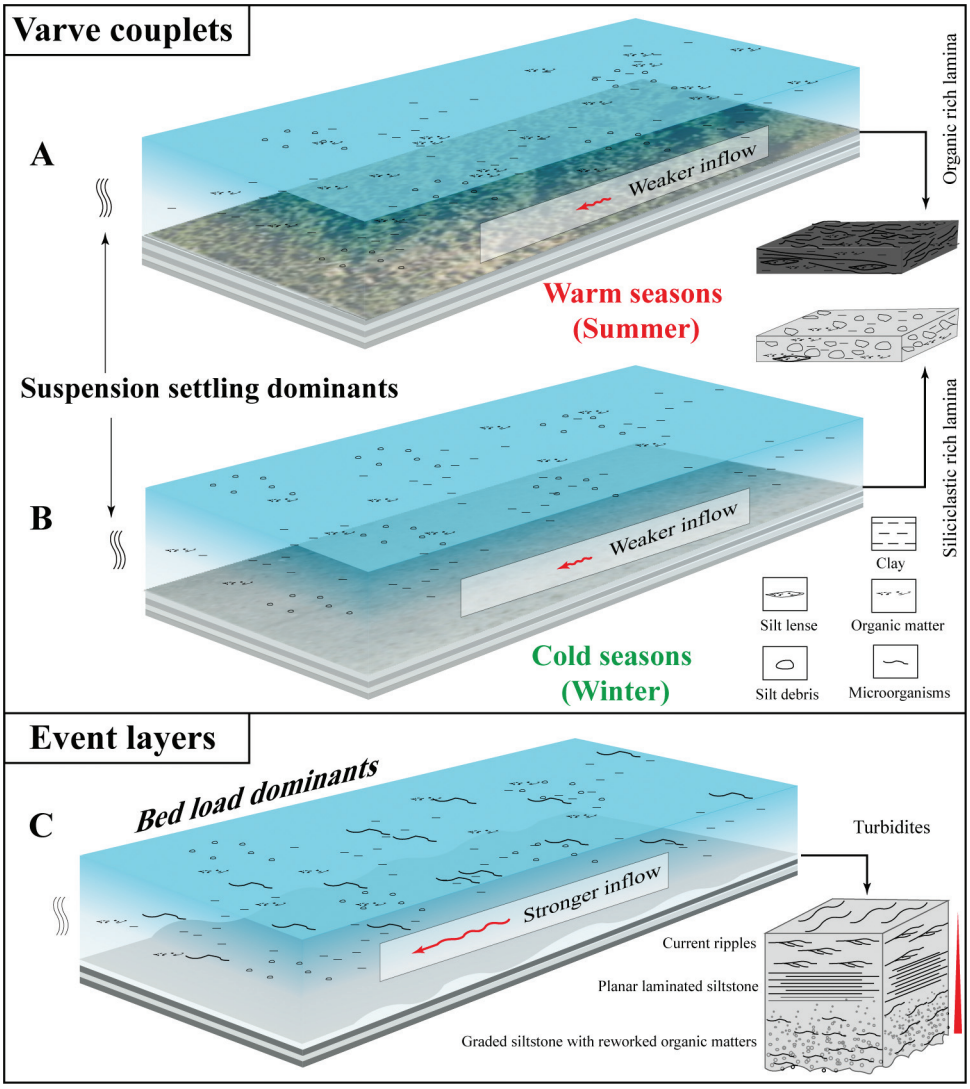

Fig. 7. Depositional model of the striped shale. A) The deposition of couplet from gray to black organic-rich mudstone (Mf 2), from which the organic-rich sublamina (biofilm dominated) are tend to deposit in warm seasons (for example, summer) with more solar radiation; B) While the siliciclastic-rich sublamina are tend to deposit in cold seasons (for example, winter) with less solar radiation; C) The deposition of light-gray to gray siltstone (Mf 1) tend to be event layer.

temperature is larger than that in winter in the Northern Hemisphere, and benthic microbial mats flourish during summer and are easy to wither in winter (Schieber and others, 2007; Ma and others, 2017). We propose that this could happen in the Early Cretaceous following the same processes (figs. 7A and 7B).

Third, the sedimentation rates may also support our varve explanation. For the sedimentation rates of the Yixian Formation, Smith and others proposed that the rate of sedimentation was as high as 500 to 2000 μm/year (Smith and others, 1995). Zhu and others suggested the lacustrine sedimentary rate is no less than 20 μm/year (Zhu and others, 2007). Chang and others argued that the rate of accumulation to be 22 to

250 μm/year (Chang and others, 2009). Zhang and Sha found the average varve thickness varies from 200 to 700 μm (Zhang and Sha, 2012). Finally, according to Hethke and others (2013), the varve thickness in Sihetun is from 37 to 383 μm/year. These indicate that the sedimentation rate of the majority of the mudstones and shales in the Yixian Formation is approximately 20 to 2000 μm/year, which means if we assume the lowerbound sedimentation rate (20 um/yr) and the upperbound (2000 um/yr), the 3.3 cm varved interval (362 varve couplets) in this paper could comprise 1650 and 17 varve couplets, respectively.

As for the depositional environment, we suggest that Mf 2 likely formed under subtidal environments or deeper in the euphotic zone. Even though most varves are formed in quiet, deep or restricted environments, some studies also found varves deposited in more energetic conditions (Tang and others, 2014; Li and others, 2018). The well-preserved original morphology (figs. 3 and 5) of the biofilms suggests that the organic matter mainly originates from *in situ* burial and reworked suspension of the benthic microbial mats. Further, it appears that biofilm protection and early diagenetic processes were the most important factors for preserving these sediments (particle trapping or binding). Sometimes the microbial mats (figs. 7A and 7B, Mf 2) would be burried by a sudden influx of sediments (fig. 7C, Mf 1), causing a temporary interruption of mat growth. Following this, when the environment reaches a balance, biofilms will begin to flourish again, and such reciprocating deposition can then lead to 'striped shales' with alternating mat and event layers (Schieber and others, 2007).

LAMINA PERIODICITIES

Assuming the annual origin of the laminar couplets of Mf 2-2 in this study, power spectral analyses of the binary rank series (the binary boxcar series, triangle series and midpoint-triangle series) exhibit a periodicity of 13.8, 10.0 to 10.6, and ENSO-like signals (2–7 yrs) (fig. 8). Even though obtaining binary rank series is the most accurate reconstruction that exactly follows the field observations, it imposes strong artifacts and interference in the spectral analysis (Yao and Hinnov, 2019). From fig. 8, the binary series can artificially weaken or remove lower-frequency signals. Therefore, the gray data series and the varve thicknesses (fig. 9) of the same sample are also used to verify the results of the binary rank series. As shown in fig. 9, we found similar periodicities consistent with Schwabe sunspot cycles (10.0–10.6 year; red shaded areas), solar Hale cycles (21.9 year; green shaded areas), unknown cycles (16.5 year; blue shaded areas), which may reveal solar-like magnetic activity found by others (Qian and others, 2007), and solar Bruckner cycles (31.0–40.6 year; yellow shaded areas) (Sazonov, 1979; Raspopov and others, 2000).

Although the periods recorded by each data series are slightly different, they all record very robust quasi-decadal (~11 year) bands (figs. 8 and 9), and the ~11 yr filthering of the binary series also correspond well with the varve thickness (fig. 10). The coexistence of the inter-decadal bands (21.9 yr), multi-decadal bands (31–40.6 yr), and the decadal bands (10 to 10.6 yr) tend to be solar cycles (figs. 9I and 9J). Further, the Schwabe sunspot cycle (~11 yr) has fluctuated slightly in a range of 10.44 to 11.16 year during the last four centuries (Kane, 2002; Li and others, 2004), and in a wider range of 8.6 to 14.7 year over Earth's history (table 1). Within error, the strongest 10.0 to 10.6 to year cycles in this study are therefore proposed to be Early Cretaceous Schwabe sunspot cycles.

DEEP-TIME SOLAR CYCLES PRESERVED IN VARVES

It is well known that modern-day decadal periodic climate variations are related to solar activity (for example, Haigh, 1996; Lockwood, 2012; Solanki and others, 2013; Hathaway, 2015). Numerous solar cycles have been recognized, such as the most

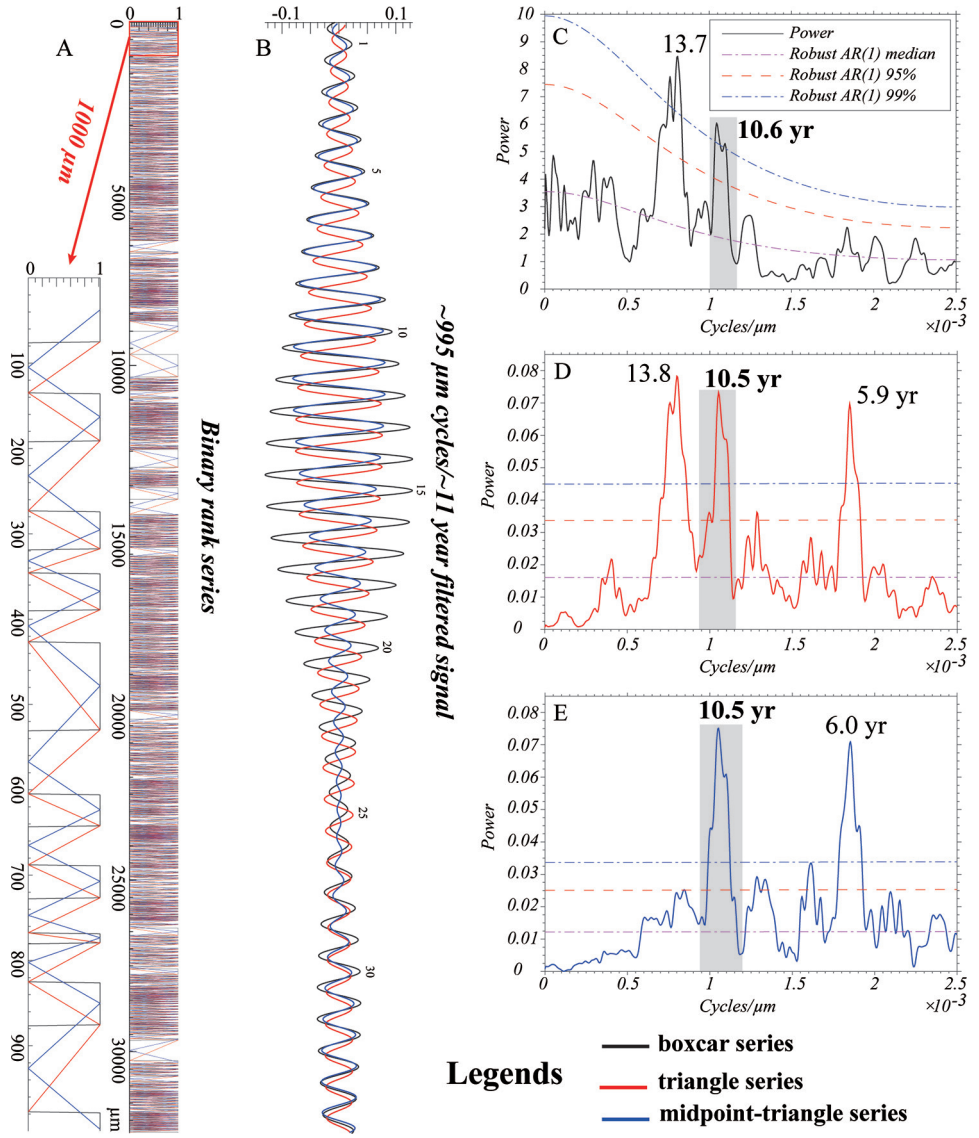

Fig. 8. Comparison of the boxcar, triangle, and midpoint-triangle series. A) Binary boxcar series, triangle series and midpoint-triangle series. B) The interpreted Schwabe sunspot cycle (~11 year) extracted with passbands of 0.001 ± 0.0001 cycles/μm. C) 2π MTM power spectral of boxcar binary series, D) triangle series and E) midpoint-triangle series, respectively. The 2π MTM with a red noise model are computed with 6500 μm window and 60 μm step. Significant peaks are labeled in year (calculated from an average couplet thickness of 90.4 μm). The shaded area in B, C and D are the filter passbands of sunspot tuning in B and fig. 9 for the three binary series. Triangle series (green curve) is phase-shifted for every cycle by a factor of π/2.

fundamental solar cycles [11-year Schwabe sunspot cycle (Schwabe, 1844), 22-year Hale cycle (Hale, 1908; Hale and others, 1919), 88-year Gleissberg cycle (Gleissberg, 1939)], as well as other solar cycles (for example, 30 to 45-year Bruckner cycle; Bruckner, 1890) introduced before. However, whether solar cycles have been persistent throughout the geological time remains uncertain. Here, to compare to our

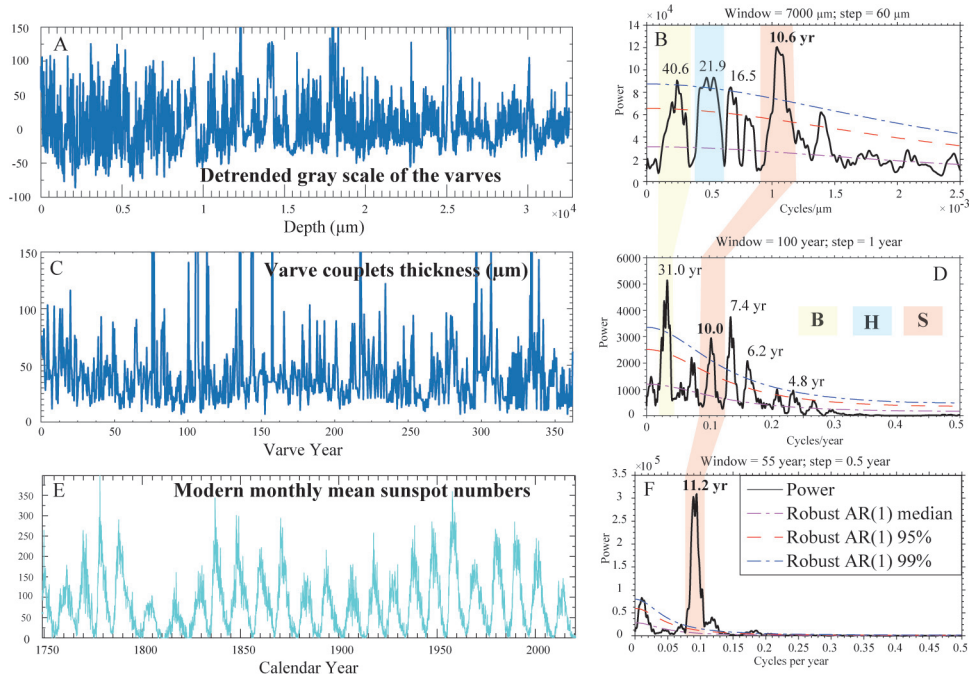

Fig. 9. Early Cretaceous and modern climate proxies and their 2π MTM spectral analytical results. A) and B) gray data series in this study and its power spectrum; C) and D) Varve thickness data series and its power spectrum; E) and F) Modern monthly mean sunspot number from 1749 to 2020 and its power spectrum, data source: WDC-SILSO, Royal Observatory of Belgium, Brussels-http://www.sidc.be/silso/datafiles. Significant peaks are labeled in year (calculated from an average couplet thickness of 90.4 μm). The shaded areas show the passbands of S: Schwabe sunspot cycles (red shaded area), H: the solar Hale cycles (blue shaded area), and B: the solar Bruckner cycles (yellow shaded area).

results and look at the consistency of sunspot cycles reported in the geologic record, we report a new compilation of solar cycle studies for deep-time varves since the Paleoproterozoic (fig. 11).

Five varved records have been identified as solar cycles in the Precambrian (fig. 11). These include: Hughes and others (2003) who recognized 9.9 to 10.7 year Schwabe sunspot cycles in rhythmically deposited argillites of a glacial lake in the Early Paleoproterozoic; Tang and others (2014) who found the first reported 9.0 to 11.7 year Schwabe sunspot cycles and 19.7 to 21.4 year Hale cycles in Mesoproterozoic marine carbonates; and Li and others (2018) who found 10 to 11.4 year Schwabe sunspot cycles and 18.9 to 25.6 Hale cycles in Neoproterozoic marine carbonate biolaminites. These solar cycles indicate that the solar activity did not change significantly during the Proterozoic Era.

At least four varve records for solar cycles have been discovered in the Paleozoic. This includes, the 8.6 to 13.7 year Schwabe sunspot cycles and 19.6 to 22.7 year Hale cycles from the Devonian (*c.* 388 Ma) low latitudes non-glacial varves (Andrews and others, 2010), the 12 year Schwabe sunspot cycles and 24 to 26 year Hale cycles in the Late Carboniferous glacial marine clastic varves (Milana and Lopez, 1998), and the 12.4 year Schwabe sunspot cycles and 24.4 year Hale cycles in the Late Carboniferous/Early Permian glacial marine clastic varves (Ernesto and Pacca, 1981).

For the Mesozoic and the Cenozoic period before the Quaternary, eight varved records for solar cycles are documented, including the 13 year Schwabe sunspot cycle, 20 year Hale cycle, 88-year Gleissberg cycle, 179 and 235 year Suess/De Vries cycles in

Fig. 10. Sunspot cycle filtering of the box, triangle and mid-point triangle series. A) Box, triangle and mid-point triangle series show a 5045-μm-long part, as shown in B; B) Filtered sunspot signals of the box (red curve), triangle series (green curve) that is phase-shifted for every cycle by a factor of π/2 (Li and others, 2018) and the mid-point triangle series (blue curve).

the Early Jurassic non-marine limestone varves (Anderson and Kirkland, 1960; Heydari and others, 1997; Dmitriev and others, 2016), the 10.3 to 10.8 year Schwabe sunspot cycles in the Late Cretaceous laminated Marca Shale of California (Davies

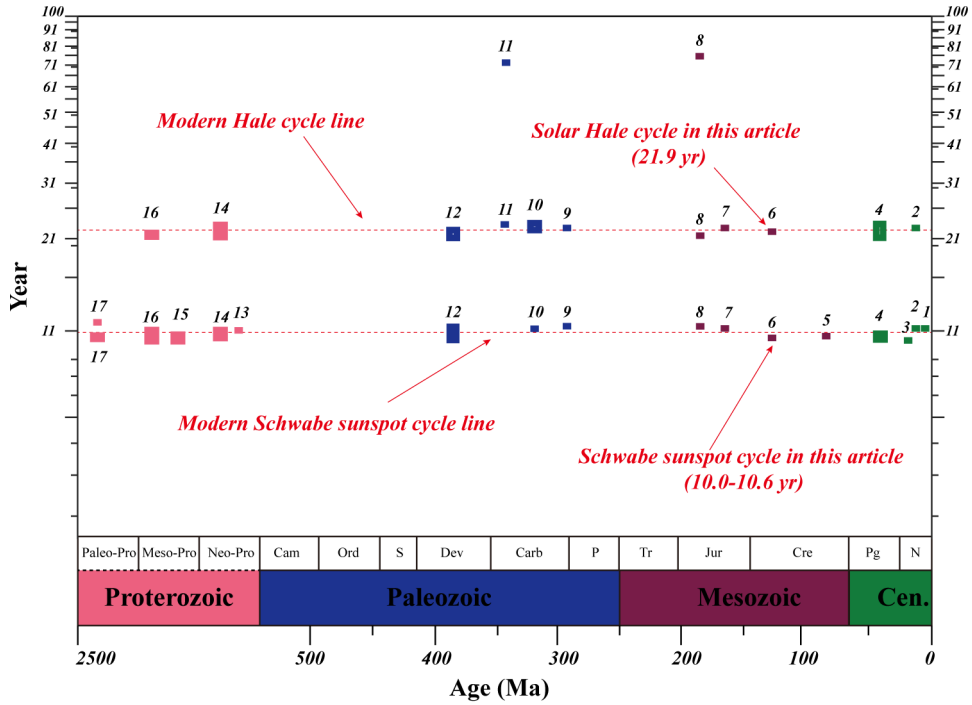

Fig. 11. Schwabe sunspot cycles, solar Hale cycles and Gleissberg cycles recorded in the Pre-Quaternary/deep-time varves and this study. The small colored rectangle in the picture represents rough time span of its periodicities and its approximate location in the geological time scale, numbers above the respective columns are connected with the citations given in table 1.

and others, 2012), the 10 year Schwabe sunspot cycle in the latest Messinian (Miocene) marine mixed varves (Cosentino and others, 2005), the 12 year Schwabe sunspot cycle and 24 year Hale cycles in the latest Miocene and earliest Pliocene sinkhole lake clastic varves (Shunk and others, 2009), and the 12 year Schwabe sunspot cycles in lacustrine biogenic varves from the Pliocene Villarroya Pliocene Basin (Spain) (Muñoz and others, 2002; Gauthier and Muñoz, 2009). From the varve data base created by previous work (Ojala and others, 2012; Zolitschka and others, 2015; Ramisch and others, 2020), it has been demonstrated that Quaternary varves are abundant in high and low latitude areas across continents and oceans, and the great wealth of varve records about solar cycles attest to the stability of the solar cycles during the Quaternary.

This research reports the first continental varve recorded solar cycles in Asia in the Early Cretaceous and fills the gap during this greenhouse interval (fig. 11). We consider that mat growth in Early Cretaceous Northern Liaoning was potentially affected by seasonally fluctuating climates, and it was also affected by changes in TSI caused by variance of sunspots in a longer term (11 year). Seasonally changing water depths corresponding to fluctuations in light intensities can trigger the stacked buildup of sets of dark/light laminae (Schieber and others, 2007), and modulation of the radiation reaching different hemispheres of Earth could also directly cause the microbial mats change seasonally. The modern, observational records show that TSI is in phase with monthly mean sunspot numbers (Solanki and others, 2013). Since the small changes in energy output over 11 year sunspot cycle can be amplified to a level sufficient to produce changes in weather and climate (Cubasch and Voss, 2000;

Higginson and others, 2004; Moore and others, 2006; Gray and others, 2010; Lockwood, 2012; Solanki and others, 2013), it can be theorized that more sunspot means more TSI acts on Earth's ecosystem, thereby enhancing biological photosynthesis, and finally producing thicker biofilms, while less sunspots lead to thinner biofilms. This notion is further verified by an ~11-year cycle in the laminar couplets of Mf 2 with thicker biofilms tending to occur in the middle of the phase of the ~11-year filtered wave (fig. 10).

Although there are missing examples of solar cycles in the Cambrian, Ordovician, Silurian, and Triassic periods, combined with previously published records and the results of this study, it can be inferred that the Schwabe sunspot cycles and the solar Hale cycles are likely persistent throughout geological time (fig. 11). This further proves that solar variance could have been an important factor in regulating the photosystem (Hawes and others, 2001; Hawes and others, 2014; Hawes and others, 2016) and affecting the Earth's climate (Reid, 2000; Lean and Rind, 2001; Haigh, 2003; Biktash, 2019) throughout geological time (table 1). The stable phases of solar cycles supports the presumption that solar variability will continue to influence earth's climate in the future (Lean and Rind, 1999; Bond and others, 2001; Lean, 2010).

CONCLUSIONS

Based on detailed petrological analysis, we proposed a depositional model for the striped shale of the Third Member of the Yixian Formation in Xiushui Basin, NE China. The laminations are presented as rhythmical couplets of biofilms and siliciclastic-rich sublaminae are varves and represent annual laminations. The changes from siliciclastic-rich sublamina to biofilms indicate seasonal growth and withering of the microbial mats during the warm season (for example, summer) and cold season (for example, winter), respectively.

Power spectral analyses of the binary rank series (the binary boxcar series, triangle series and midpoint-triangle series), the gray data series and varve thickness of a well laminated mudstone interval (~3.3 cm in length) showed bands consistent with solar cycles, such as the Schwabe sunspot cycles (10.0–10.6 year), the solar Hale cycles (21.9 year) and solar Bruckner cycles (31.0–40.6 year). The Schwabe sunspot cycles (10.0–10.6 year; figs. 8 and 9) are very robust, indicating solar activity has influenced the growth of biofilms. We postulate that, like today, solar activity may have influenced Earth's climate through total solar irradiance (TSI) in the Early Cretaceous. In this conceptual model, less sunspots can cause less TSI, resulting in thinner biofilms and thicker siliciclastic-rich sublaminae. Although the records are still incomplete through geologic history, emerging evidence suggests that the periodicities of the Schwabe sunspot cycles and solar Hale cycles have been persistent through much of the last 1 billion years or longer.

ACKNOWLEDGMENTS

The authors acknowledge the recommendations of Prof. Brad Sageman and the reviews by two anonymous reviewers. This work was supported by the National Natural Science Foundation of China (41972096, 41790452), the Fundamental Research Funds for the Central Universities of China (2652018119) and the "111" project (B20011). D. E. I. was supported by the UC Berkeley Miller Research Institute and UC President's Postdoctoral Fellowships.

REFERENCES

Algeo, T. J., and Woods, A. D., 1994, Microstratigraphy of the Lower Mississippian Sunbury Shale: A record of solar-modulated climatic cyclicity: Geology, v. 22, n. 9, p. 795–798, https://doi.org/10.1130/0091-7613(1994)022<0795:MOTLMS>2.3.CO;2

Anderson, R. Y., and Dean, W. E., 1988, Lacustrine varve formation through time: Palaeogeography, Palaeoclimatology, Palaeoecology, v. 62, n. 1–4, p. 215–235, https://doi.org/10.1016/0031-0182(88)90055-7

Anderson, R. Y., and Kirkland, D. W., 1960, Origin, varves, and cycles of Jurassic Todilto formation, New Mexico: AAPG Bulletin, v. 44, n. 1, p. 37–52, https://doi.org/10.1306/0BDA5F75-16BD-11D7-8645000102C1865D

Andrews, S. D., Trewin, N. H., Hartley, A. J., and Weedon, G. P., 2010, Solar variance recorded in lacustrine deposits from the Devonian and Proterozoic of Scotland: Journal of the Geological Society, v. 167, p. 847–856, https://doi.org/10.1144/0016-76492009-105

Arenas, C., and Jones, B., 2017, Temporal and environmental significance of microbial lamination: Insights from Recent fluvial stromatolites in the River Piedra, Spain: Sedimentology, v. 64, n. 6, p. 1597–1629, https://doi.org/10.1111/sed.12365

Biktash, L. Z., 2019, Influence of Total Solar Irradiance on the Earth's Climate: Geomagnetism and Aeronomy, v. 59, p. 368–373, https://doi.org/10.1134/S0016793219030058

Bond, G., Kromer, B., Beer, J., Muscheler, R., Evans, M. N., Showers, W., Hoffmann, S., Lotti-Bond, R., Hajdas, I., and Bonani, G., 2001, Persistent Solar Influence on North Atlantic Climate During the Holocene: Science, v. 294, n. 5549, p. 2130–2136, https://doi.org/10.1126/science.1065680

Bouma, A. H., 1964, Turbidites: Developments in Sedimentology: Elsevier, v. 3, p. 247–256, https://doi.org/10.1016/S0070-4571(08)70967-1

Bruckner, E., 1890, Klima-Schwankungen seit 1700, nebst Bemerkungen über die Klimaschwankungen der Diluvialzeit; Wien, Austria, E. Hölzel, v. 4, 325 p.

Cao, H. H., ms, 2013, Geochronology and geochemistry of the Late Paleozoic-Early Mesozoic igneous rock in the eastern segment of the eastern margin of the North China block: Ph.D. thesis, Jilin University, Jilin, China, 171 p. (in Chinese with English abstract).

Chang, M. M., Zhang, J., and Miao, D., 2006, A lamprey from the Cretaceous Jehol biota of China: Nature, v. 441, p. 972–974, https://doi.org/10.1038/nature04730

Chang, S.-c., Zhang, H., Renne, P. R., and Fang, Y., 2009, High-precision $^{40}Ar/^{39}Ar$ age for the Jehol Biota: Palaeogeography, Palaeoclimatology, Palaeoecology, v. 280, p. 94–104, https://doi.org/10.1016/j.palaeo.2009.06.021

Chen, S., Gong, F., and Yang, J., 2016, Progress and Orientation of the Project about Fundamental Geological Survey on Oil and Gas Resources in the Periphery Area of Songliao Basin: Geological Survey of China, v. 3, p. 1–9 (in Chinese with English abstract).

Cosentino, D., Cipollari, P., Lo Mastro, S., and Giampaolo, C., 2005, High-frequency cyclicity in the latest Messinian Adriatic foreland basin: Insight into palaeoclimate and palaeoenvironments of the Mediterranean Lago-Mare episode: Sedimentary Geology, v. 178, n. 1–2, p. 31–53, https://doi.org/10.1016/j.sedgeo.2005.03.010

Cubasch, U., and Voss, R., 2000, The influence of total solar irradiance on climate: Space Science Reviews, v. 94, p. 185–198, https://doi.org/10.1023/A:1026719322987

Davies, A., Kemp, A. E. S., Weedon, G. P., and Barron, J. A., 2012, El Niño–Southern Oscillation variability from the Late Cretaceous Marca Shale of California: Geology, v. 40, n. 1, p. 15–18, https://doi.org/10.1130/G32329.1

de Geer, G., 1912, Greochronologie der letzten 12000 Jahre: Geologische Rundschau, v. 3, p. 457–471, https://doi.org/10.1007/BF01802565

Ding, Q., Chen, S., Li, X., Li, W., and Yao, Y., 2017, Spore-Pollen assemblages of Xiu D1 well in Xiushui basin, northern Liaoning Province and their stratigraphic singnificance: Geological Bulletin of China, v. 36, p. 1305–1318 (in Chinese with English abstract).

Ding, Q., Chen, S., Li, X., Li, W., Yao, Y., Zhang, J., and Sun, S., 2019, Geological characteristics and oil-bearing prospect of Lower Cretaceous in Xiushui Basin of northern Liaoning Province: Geological Survey of China, v. 6, p. 14–21 (in Chinese with English abstract).

Ding, Q., Li, X., Li, W., Chen, S., Zhang, J., and Sun, S., 2020, Geophysical response of the stratigraphic division of yixian formation in xiushui basin, northern liaoning province: Geology and resources, v. 29, p. 44–52+6 (in Chinese with English abstract).

Dmitriev, P. B., Dergachev, V. A., Tyasto, M. I., and Blagoveshchenskaya, E. E., 2016, Cycles revealed in Jurassic paleoclimatic data (*ca.* 200–145 Ma BP): Geomagnetism and Aeronomy, v. 56, p. 914–919, https://doi.org/10.1134/S0016793216070045

Ernesto, M., and Pacca, I. G., 1981, Spectral analysis of Permocarboniferous geomagnetic variation data from glacial rhythmites: Geophysical Journal International, v. 67, n. 3, p. 641–647, https://doi.org/10.1111/j.1365-246X.1981.tb06943.x

Francus, P., Ridge, J. C., and Johnson, M. D., 2013, The rise of varves: GFF, v. 135, n. 3–4, p. 229–230, https://doi.org/10.1080/11035897.2013.833548

Gauthier, A., and Muñoz, A., 2009, Seasonal sedimentation in the Pliocene Villarroya Lake (N Spain) inferred from pollen analysis: Sedimentary Geology, v. 222, n. 1–2, p. 111–123, https://doi.org/10.1016/j.sedgeo.2009.06.008

Gilbert, G. K., 1895, Sedimentary measurement of Cretaceous time: The Journal of Geology, v. 3, n. 2, p. 121–127, https://doi.org/10.1086/607150

Gleissberg, W., 1939, A long-periodic fluctuation of the sun-spot numbers: The Observatory, v. 62, p. 158–159.

Gray, L. J., Beer, J., Geller, M., Haigh, J. D., Lockwood, M., Matthes, K., Cubasch, U., Fleitmann, D., Harrison, G., Hood, L., Luterbacher, J., Meehl, G. A., Shindell, D., van Geel, B., and White, W., 2010, Solar influences on climate: Reviews of Geophysics, v. 48. n. 4, p. RG4001, https://doi.org/10.1029/2009RG000282

Haigh, J. D., 1996, The impact of solar variability on climate: Science, v. 272, n. 5264, p. 981–984, https://doi.org/10.1126/science.272.5264.981

Haigh, J. D., 2003, The effects of solar variability on the Earth's climate: Philosophical Transactions of the Royal Society of London, Series A: Mathematical, Physical and Engineering Sciences, v. 361, n. 1802, p. 95–111, https://doi.org/10.1098/rsta.2002.1111

Hale, G. E., 1908, On the Probable Existence of a Magnetic Field in Sun-Spots: The Astrophysical Journal, v. 28, p. 315, https://doi.org/10.1086/141602

Hale, G. E., Ellerman, F., Nicholson, S. B., and Joy, A. H., 1919, The magnetic polarity of Sun-Spots: The Astrophysical Journal, v. 49, p. 153, https://doi.org/10.1086/142452

Hathaway, D. H., 2015, The Solar Cycle: Living Reviews in Solar Physics, v. 12., p. 4, https://doi.org/10.1007/lrsp-2015-4

Hawes, I., Giles, H., and Doran, P. T., 2014, Estimating photosynthetic activity in microbial mats in an ice-covered Antarctic lake using automated oxygen microelectrode profiling and variable chlorophyll fluorescence: Limnology and Oceanography, v. 59, n. 3, p. 674–688, https://doi.org/10.4319/lo.2014.59.3.0674

Hawes, I., Jungblut, A. D., Obryk, M. K., and Doran, P. T., 2016, Growth dynamics of a laminated microbial mat in response to variable irradiance in an Antarctic lake: Freshwater Biology, v. 61, n. 4, p. 396–410, https://doi.org/10.1111/fwb.12715

Hawes, I., Moorhead, D., Sutherland, D., Schmeling, J., and Schwarz, A.-M., 2001, Benthic primary production in two perennially ice-covered Antarctic lakes: patterns of biomass accumulation with a model of community metabolism: Antarctic Science, v. 13, n. 1, p. 18–27, https://doi.org/10.1017/S0954102001000049

Hethke, M., Fürsich, F. T., Jiang, B., and Pan, Y., 2013, Seasonal to sub-seasonal palaeoenvironmental changes in Lake Sihetun (Lower Cretaceous Yixian Formation, NE China): International Journal of Earth Sciences, v. 102, p. 351–378, https://doi.org/10.1007/s00531-012-0799-7

Heydari, E., Wade, W. J., and Anderson, L. C., 1997, Depositional environments, organic carbon accumulation, and solar-forcing cyclicity in smackover formation lime mudstones, northern Gulf Coast: AAPG Bulletin-American Association of Petroleum Geologists, v. 81, n. 5, p. 760–774, https://doi.org/10.1306/522B4839-1727-11D7-8645000102C1865D

Higginson, M. J., Altabet, M. A., Wincze, L., Herbert, T. D., and Murray, D. W., 2004, A solar (irradiance) trigger for millennial-scale abrupt changes in the southwest monsoon?: Paleoceanography, v. 19, p. PA3015, https://doi.org/10.1029/2004PA001031

Howard-Williams, C., Schwarz, A.-M., Hawes, I., and Priscu, J. C., 2013, Optical Properties of the Mcmurdo Dry Valley Lakes, Antarctica: Ecosystem Dynamics in a Polar Desert: The Mcmurdo Dry Valleys, Antarctica, Antarctic Research Series: Washington, DC, American Geophysical Union, v. 72, p. 189–203, https://doi.org/10.1029/AR072p0189

Hughes, G. B., Giegengack, R., and Kritikos, H. N., 2003, Modern spectral climate patterns in rhythmically deposited argillites of the Gowganda Formation (Early Proterozoic), southern Ontario, Canada: Earth and Planetary Science Letters, v. 207, n. 1–4, p. 13–22, https://doi.org/10.1016/S0012-821X(02)01155-X

Jiang, B., Fürsich, F. T., and Hethke, M., 2012, Depositional evolution of the Early Cretaceous Sihetun Lake and implications for regional climatic and volcanic history in western Liaoning, NE China: Sedimentary Geology, v. 257–260, p. 31–44, https://doi.org/10.1016/j.sedgeo.2012.02.007

Kane, R. P., 2002, Some implications using the group sunspot number reconstruction: Solar Physics, v. 205, p. 383–401, https://doi.org/10.1023/A:1014296529097

Korn, H., and Martin, H., 1951, Cyclic sedimentation in varved sediments of the Nama system in South-West Africa: South African Journal of Geology, v. 54, n. 1, p. 65–67.

Lean, J., 2010, Cycles and trends in solar irradiance and climate: Wiley interdisciplinary reviews: climate change, v. 1, n. 1, p. 111–122, https://doi.org/10.1002/wcc.18

Lean, J., and Rind, D., 1999, Evaluating sun-climate relationships since the Little Ice Age: Journal of Atmospheric and Solar-Terrestrial Physics, v. 61, n. 1–2, p. 25–36, https://doi.org/10.1016/S1364-6826(98)00113-8

Lean, J., and Rind, D., 2001, Earth's response to a variable Sun: Science, v. 292, n. 5515, p. 234–236, https://doi.org/10.1126/science.1060082

Li, K., Su, T., and Liang, H., 2004, Periodicity of sunspot activity in the modern solar cycles: Chinese Science Bulletin, v. 49, p. 2247–2252, https://doi.org/10.1007/BF03036889

Li, M., Hinnov, L., and Kump, L., 2019a, Acycle: Time-series analysis software for paleoclimate research and education: Computers & Geosciences, v. 127, p. 12–22, https://doi.org/10.1016/j.cageo.2019.02.011

Li, P., Tang, D., Shi, X., Jiang, G., Zhao, X., Zhou, X., Wang, X., and Chen, X., 2018, Sunspot cycles recorded in siliciclastic biolaminites at the dawn of the Neoproterozoic Sturtian glaciation in South China: Precambrian Research, v. 315, p. 75–91, https://doi.org/10.1016/j.precamres.2018.07.018

Li, W., Li, X., Ding, Q., Chen, S., and Zhang, J., 2019b, Geochemical characteristics and paleoenvironment of Cretaceous Jiufotang Formation in Xiushui Basin,northern Liaoning: Global Geology, v. 38, p. 154–161 (in Chinese with English abstract).

Li, Y., Cao, X., Wang, L., and Song, Z., 2017, The paleoclimate significance of hydrogen isotopic composition of individual hydrocarbon compounds in the Early Cretaceous Yixian Formation sediments from western Liaoning: Earth Science Frontiers, v. 24, p. 416–426 (in Chinese with English abstract).

Lockwood, M., 2012, Solar Influence on Global and Regional Climates: Surveys in Geophysics, v. 33, p. 503–534, https://doi.org/10.1007/s10712-012-9181-3

Luthardt, L., and Rößler, R., 2017, Fossil forest reveals sunspot activity in the early Permian: REPLY: Geology, v. 45, n. 10, p. e428, https://doi.org/10.1130/G39607Y.1

Ma, J., Wu, C., Wang, Y., Wang, J., Fang, Y., Zhu, W., Zhai, L., and Zhou, T., 2017, Paleoenvironmental reconstruction of a saline lake in the Tertiary: Evidence from aragonite laminae in the northern Tibet Plateau: Sedimentary Geology, v. 353, p. 1–12, https://doi.org/10.1016/j.sedgeo.2017.03.002

Meyers, S., 2014, Astrochron: An R package for astrochronology, https://cran.r-project.org/package=astrochron
Milana, J. P., and Lopez, S., 1998, Solar cycles recorded in Carboniferous glacimarine rhythmites (Western Argentina): relationships between climate and sedimentary environment: Palaeogeography, Palaeoclimatology, Palaeoecology, v. 144, n. 1–2, p. 37–63, https://doi.org/10.1016/S0031-0182(96)00037-5
Moore, J., Grinsted, A., and Jevrejeva, S., 2006, Is there evidence for sunspot forcing of climate at multi-year and decadal periods?: Geophysical Research Letters, v. 33, n. 17, p. L17705, https://doi.org/10.1029/2006GL026501
Muñoz, A., Ojeda, J., and Sánchez-Valverde, B., 2002, Sunspot-like and ENSO/NAO-like periodicities in lacustrine laminated sediments of the Pliocene Villarroya Basin (La Rioja, Spain): Journal of Paleolimnology, v. 27, p. 453–463, https://doi.org/10.1023/A:1020319923164
Noffke, N., 2010, Geobiology: Microbial mats in sandy deposits from the Archean Era to today: Springer Science & Business Media, 200 p.
Ojala, A. E. K., Francus, P., Zolitschka, B., Besonen, M., and Lamoureux, S. F., 2012, Characteristics of sedimentary varve chronologies - A review: Quaternary Science Reviews, v. 43, p. 45–60, https://doi.org/10.1016/j.quascirev.2012.04.006
Pan, Y., Sha, J., Fürsich, F. T., Wang, Y., and Zhang, X., And Yao, X., 2012, Dynamics of the lacustrine fauna from the Early Cretaceous Yixian Formation, China: implications of volcanic and climatic factors: Lethaia, v. 45, p. 299–314, https://doi.org/10.1111/j.1502-3931.2011.00284.x
Pinckney, J., Paerl, H., and Fitzpatrick, M., 1995, Impacts of seasonality and nutrients on microbial mat community structure and function: Marine Ecology Progress Series, v. 123, p. 207–216, https://doi.org/10.3354/meps123207
Qian, S.-B., Yuan, J.-Z., Soonthornthum, B., Zhu, L.-Y., He, J.-J., and Yang, Y.-G., 2007, AD cancri: a shallow contact solar-type eclipsing binary and evidence for a dwarf third component and a 16 year magnetic cycle: The Astrophysical Journal, v. 671, n. 1, p. 811, https://doi.org/10.1086/522421
Ramisch, A., Brauser, A., Dorn, M., Blanchet, C., Brademann, B., Köppl, M., Mingram, J., Neugebauer, I., Nowaczyk, N., Ott, F., Pinkerneil, S., Plessen, B., Schwab, M. J., Tjallingii, R., and Brauer, A., 2020, VARDA (VArved sediments DAtabase) - providing and connecting proxy data from annually laminated lake sediments: Earth System Science Data, v. 12, n. 3, p. 2311–2332, https://doi.org/10.5194/essd-12-2311-2020
Raspopov, O. M., Shumilov, O. I., Kasatkina, E. A., Turunen, E., and Lindholm, M., 2000, 35-year Climatic Bruckner Cycle – Solar Control of Climate Variability?: The solar cycle and terrestrial climate, Solar and space weather Euroconference, v. 463, p. 517.
Reid, G. C., 2000, Solar variability and the Earth's climate: Introduction and overview: Space Science Reviews, v. 94, p. 1–11, https://doi.org/10.1023/A:1026797127105
Sazonov, B., 1979, Brückner cycle of droughts: Criterions and characteristics of droughts phenomena in USSR, Hydrometeoizdat, Leningrad, p. 82–92.
Schieber, J., 1986, The possible role of benthic microbial mats during the formation of carbonaceous shales in shallow Mid-Proterozoic basins: Sedimentology, v. 33, n. 4, p. 521–536. https://doi.org/10.1111/j.1365-3091.1986.tb00758.x
Schieber, J., Bose, P. K., Eriksson, P., Banerjee, S., Sarkar, S., Altermann, W., and Catuneanu, O., 2007, Atlas of microbial mat features preserved within the siliciclastic rock record, v. 2: Amsterdam, the Netherlands, Elsevier Science, 324 p.
Schimmelmann, A., Lange, C. B., Schieber, J., Francus, P., Ojala, A. E. K., and Zolitschka, B., 2016, Varves in marine sediments: A review: Earth-Science Reviews, v. 159, p. 215–246, https://doi.org/10.1016/j.earscirev.2016.04.009
Schwabe, H., 1844, Sonnenbeobachtungen im Jahre 1843. Von Herrn Hofrath Schwabe in Dessau: Astronomische Nachrichten, v. 21, n. 15, p. 233, https://doi.org/10.1002/asna.18440211505
Sha, J., 2007, Cretaceous stratigraphy of northeast China: non-marine and marine correlation: Cretaceous Research, v. 28, n. 2, p. 146–170, https://doi.org/10.1016/j.cretres.2006.12.002
Shanmugam, G., 2021, Deep-Water Processes and Deposits: Encyclopedia of Geology, p. 965–1009, https://doi.org/10.1016/B978-0-12-409548-9.12541-2
Shunk, A. J., Driese, S. G., and Dunbar, J. A., 2009, Late Tertiary paleoclimatic interpretation from lacustrine rhythmites in the Gray Fossil Site, northeastern Tennessee, USA: Journal of Paleolimnology, v. 42, p. 11–24, https://doi.org/10.1007/s10933-008-9244-0
Smith, P. E., Evensen, N. M., York, D., Chang, M.-M., Jin, F., Li, J.-L., Cumbaa, S., and Russell, D., 1995, Dates and rates in ancient lakes: ^{40}Ar-^{39}Ar evidence for an Early Cretaceous age for the Jehol Group, northeast China: Canadian Journal of Earth Sciences, v. 32, n. 9, p. 1426–1431, https://doi.org/10.1139/e95-115
Solanki, S. K., Krivova, N. A., and Haigh, J. D., 2013, Solar irradiance variability and climate: Annual Review of Astronomy and Astrophysics, v. 51, p. 311–351, https://doi.org/10.1146/annurev-astro-082812-141007
Spychala, Y. T., Hodgson, D. M., Prélat, A., Kane, I. A., Flint, S. S., and Mountney, N. P., 2017, Frontal and Lateral Submarine Lobe Fringes: Comparing Sedimentary Facies, Architecture and Flow Processes: Journal of Sedimentary Research, v. 87, n. 1, p. 75–96, https://doi.org/10.2110/jsr.2017.2
Stow, D. A. V., and Piper, D. J. W., 1984, Deep-water fine-grained sediments: facies models: Geological Society, London, Special Publications, v. 15, n. 1, p. 611–646, https://doi.org/10.1144/GSL.SP.1984.015.01.38
Sutherland, D. L., and Hawes, I., 2009, Annual growth layers as proxies of past growth conditions for benthic microbial mats in a perennially ice-covered Antarctic lake: Fems Microbiology Ecology, v. 67, n. 2, p. 279–292, https://doi.org/10.1111/j.1574-6941.2008.00621.x

Talling, P. J., Masson, D. G., Sumner, E. J., and Malgesini, G., 2012, Subaqueous sediment density flows: Depositional processes and deposit types: Sedimentology, v. 59, n. 7, p. 1937–2003, https://doi.org/10.1111/j.1365-3091.2012.01353.x

Tang, D., Shi, X., and Jiang, G., 2014, Sunspot cycles recorded in Mesoproterozoic carbonate biolaminites: Precambrian Research, v. 248, p. 1–16, https://doi.org/10.1016/j.precamres.2014.04.009

Thackeray, J. F., 2002, Long-term correlation between tree rings and sunspot numbers: South African Journal of Science, v. 98, n. 1, p. 104.

Tierney, J. E., Poulsen, C. J., Montanez, I. P., Bhattacharya, T., Feng, R., Ford, H. L., Hönisch, B., Inglis, G. N., Petersen, S. V., Sagoo, N., Tabor, C. R., Thirumalai, K., Zhu, J., Burls, N. J., Foster, G. L., Godderis, Y., Huber, B. T., Ivany, L. C., Turner, S. K., Lunt, D. J., McElwain, J. C., Mills, B. J. W., Otto-Bliesner, B. L., Ridgwell, A., and Zhang, Y. G., 2020, Past climates inform our future: Science, v. 370, n. 6517, p. eaay3701, https://doi.org/10.1126/science.aay3701

Villbrandt, M., Krumbein, W. E., and Stal, L. J., 1991, Diurnal and seasonal variations of nitrogen fixation and photosynthesis in cyanobacterial mats: Plant and Soil, v. 137, p. 13–16, https://doi.org/10.1007/BF02187426

Wang, C., Scott, R. W., Wan, X., Graham, S. A., Huang, Y., Wang, P., Wu, H., Dean, W. E., and Zhang, L., 2013, Late Cretaceous climate changes recorded in Eastern Asian lacustrine deposits and North American Epieric sea strata: Earth-Science Reviews, v. 126, p. 275–299, https://doi.org/10.1016/j.earscirev.2013.08.016

Weedon, G. P., 2003, Time-series analysis and cyclostratigraphy: examining stratigraphic records of environmental cycles; Cambridge University Press, 274 p., https://doi.org/10.1017/CBO9780511535482

Yang, T., Cao, Y., Liu, K., Tian, J., Carlos, Z., and Wang, Y., 2020, Gravity-flow deposits caused by different initiation processes in a deep-lake system: AAPG Bulletin, v. 104, n. 7, p. 1463–1499, https://doi.org/10.1306/03172017081

Yao, X., and Hinnov, L. A., 2019, Advances in characterizing the cyclostratigraphy of binary chert-mudstone lithologic successions, Permian (Roadian-lower Capitanian), Chaohu, Lower Yangtze, South China: Palaeogeography, Palaeoclimatology, Palaeoecology, v. 528, p. 258–271, https://doi.org/10.1016/j.palaeo.2019.05.004

Yao, X., Zhou, Y., and Hinnov, L. A., 2015, Astronomical forcing of a Middle Permian chert sequence in Chaohu, South China: Earth and Planetary Science Letters, v. 422, p. 206–221, https://doi.org/10.1016/j.epsl.2015.04.017

Yao, Y., Li, X., Si, J., Ding, Q., and Li, W., 2018, Evalution of the source rocks from X-D1 well in Xiushui Basin, Northern Liaoning provincce: Geology and Resources, v. 27, p. 186–191 (in Chinese with English abstract).

Zhang, X., and Sha, J., 2012, Sedimentary laminations in the lacustrine Jianshangou Bed of the Yixian Formation at Sihetun, western Liaoning, China: Cretaceous Research, v. 36, p. 96–105, https://doi.org/10.1016/j.cretres.2012.02.010

Zhou, Z., Barrett, P. M., and Hilton, J., 2003, An exceptionally preserved Lower Cretaceous ecosystem: Nature, v. 421, p. 807–814, https://doi.org/10.1038/nature01420

Zhu, R., Pan, Y., Shi, R., Liu, Q., and Li, D., 2007, Palaeomagnetic and $^{40}Ar/^{39}Ar$ dating constraints on the age of the Jehol Biota and the duration of deposition of the Sihetun fossil-bearing lake sediments, northeast China: Cretaceous Research, v. 28, n. 2, p. 171–176. https://doi.org/10.1016/j.cretres.2006.06.003

Zhu, R., Shao, J., Pan, Y., Shi, R., Shi, G., and Li, D., 2002, Paleomagnetic data from Early Cretaceous volcanic rocks of West Liaoning: Evidence for intracontinental rotation: Chinese Science Bulletin, v. 47, p. 1832–1837, https://doi.org/10.1007/BF03183852

Zolitschka, B., Francus, P., Ojala, A. E. K., and Schimmelmann, A., 2015, Varves in lake sediments - a review: Quaternary Science Reviews, v. 117, p. 1–41, https://doi.org/10.1016/j.quascirev.2015.03.019